


Mobility edges in non-Hermitian models with slowly varying quasiperiodic disorderQiyun Tang and Yan He ^{*}*College of Physics, Sichuan University, Chengdu, Sichuan 610064, China*

(Received 4 March 2024; revised 3 June 2024; accepted 5 June 2024; published 20 June 2024)

We investigate the appearance of mobility edges in a one-dimensional non-Hermitian tight-binding model with alternating hopping constants and slowly varying quasiperiodic on-site potentials. Due to the presence of a slowly varying exponent, the parity-time (PT) symmetry of this model is broken and its spectra are complex. It is found that the spectrum of this model can be divided into three different types of patterns depending on the magnitude of the quasiperiodic potential. As the amplitude of the potential increases from small to large, the initially well-defined mobility edges become blurred gradually and then eventually disappear for large-enough potential. This behavior of mobility edges is also confirmed by a detailed study of the winding number of complex spectra of this non-Hermitian model.

DOI: [10.1103/PhysRevB.109.224204](https://doi.org/10.1103/PhysRevB.109.224204)**I. INTRODUCTION**

The phenomena of disorders have been extensively studied in condensed matter physics. It is well known that in three-dimensional systems, strong-enough disorders will make the wave functions of the system localized, which is the famous Anderson localization [1–3]. When the disorders are not very strong, the extended and localized states coexist in the spectra and they are usually separated by the mobility edges [4]. In the subsequent developments, people tried to search for the mobility edges in low-dimensional systems but did not succeed. The reason is that at low dimensions even infinitesimally weak disorders can drive the whole spectra to complete localizations.

Due to these failures, people turned to one-dimensional (1D) quasiperiodic systems which possessed correlated disorders. One of the paradigmatic examples is the Aubry-Andre (AA) model [5,6], which is a 1D hopping model with incommensurate on-site potentials. One important feature of the AA model is the existence of the self-duality at certain disorder strength. When the disorder potential increases beyond this point, all the extended eigenstates suddenly turn into localized ones. Although the mobility edges are absent in the original AA model, they do exist in some generalized AA models with long-range hopping or unbounded potentials [7–10]. In these models, self-duality can also be employed to determine the exact shape of mobility edges. Later on, a large class of models with slowly varying quasiperiodic disorders [11–15] was introduced to support mobility edges. However, the self-duality is broken in these types of models.

Recent years have witnessed rapid developments in non-Hermitian physics, which has been applied to almost all aspects of condensed matter physics [16,17]. The non-Hermitian systems can display dramatically different properties in both topology and symmetry [18–23]. The early work that

generalized disorder systems to the non-Hermitian case was the Hatano-Nelson model [24,25]. After that, there appeared many works that generalized the original AA model to non-Hermitian lattices [26–35]. In most of these non-Hermitian quasiperiodic models, it was found that the extended or localized states usually corresponded to the real or complex spectra of the systems [36–41]. At the same time, the self-duality was an important tool to determine the mobility edges [31,42].

Although the non-Hermitian quasiperiodic models are widely investigated, the study of their slowly varying counterparts is relatively rare. In this paper, we present a detailed study on the non-Hermitian Su-Schrieffer-Heeger (NH-SSH) model [43] with slowly varying quasiperiodic on-site potentials. Because of the slowly varying potential, the parity-time (PT) symmetry is explicitly broken and the spectrum of this model is always complex. The property of self-duality is a signature of localization transition which is also lost in this model.

Despite the failure of self-duality, we can still semi-analytically determine the mobility edges by the so-called “energy matching method,” which we applied to Hermitian slowly vary models in our previous works [44,45]. Intuitively speaking, this method approximates the quasiperiodic model by a set of different periodic models. Then the region of extended states of the quasiperiodic model can be obtained by taking the intersection of the energy bands of all these periodic models. According to the spectra of these periodic models, we find that the mobility edges display three types of behaviors: well-defined, blurred, or completely disappeared. Since the spectrum of the above NH-SSH model is complex, we can also compute the winding number of this complex spectrum. The dependence of the winding number on the disorder potential also displays three different trends, which exactly match the three types of behaviors of mobility edges we mentioned previously.

The rest of this paper is organized as follows. In Sec. II, we introduce the non-Hermitian SSH model with slowly varying quasiperiodic disorders, which is the main focus of this paper.

^{*}Contact author: heyang_ctp@scu.edu.cn

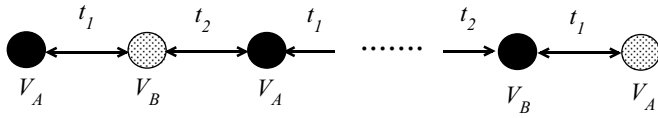


FIG. 1. The schematic figure of the model Hamiltonian of Eq. (1). The potential V_A and V_B are given in Eq. (2).

In Sec. III, we will first employ the energy matching method to qualitatively understand the spectra and mobility edges of our slowly varying quasiperiodic NH-SSH model. Then the energy spectra and inverse participate ratio (IPR) indices are numerically calculated for this model to confirm the results of the previous semi-analytical analysis. In Sec. IV, we make use of the winding number as another index to understand the behaviors of mobility edges from another angle. In the end, we briefly conclude in Sec. V.

II. SLOWLY VARYING QUASIPERIODIC NON-HERMITIAN SSH MODEL

In this section, we define the non-Hermitian SSH model with slowly varying quasiperiodic complex on-site potentials. We will focus on the energy spectrum and the behaviors of mobility edges of this model by varying its parameters. Later, we will also briefly discuss some possible generalization of this type of model. The Hamiltonian of this model can be written as

$$\hat{H} = \sum_{n=1}^{L/2} [(t_1 \hat{c}_{n,A}^\dagger \hat{c}_{n,B} + t_2 \hat{c}_{n,B}^\dagger \hat{c}_{n+1,A} + \text{H.c.}) + V_{n,A} \hat{c}_{n,A}^\dagger \hat{c}_{n,A} + V_{n,B} \hat{c}_{n,B}^\dagger \hat{c}_{n,B}]. \quad (1)$$

The schematic figure of the above model is shown in Fig. 1. Here $\hat{c}_{n,A/B}^\dagger$ ($\hat{c}_{n,A/B}$) is the fermion creation (annihilation) operator at site n and orbital A or B . L is the total number of lattices sites in the model. We impose periodic boundary condition in Eq. (1). $t_1 = t - \lambda$ and $t_2 = t + \lambda$ are the intracell and intercell hopping constants, respectively. Here $V_{n,A}$ and $V_{n,B}$ are the on-site complex quasiperiodic potential which is given by

$$V_{n,A} = V e^{i(2\pi\alpha n^v)}, \quad V_{n,B} = V e^{-i(2\pi\alpha n^v)}. \quad (2)$$

Note that $V_{n,B}$ is the complex conjugate of $V_{n,A}$. Here α is an irrational number, which introduces quasiperiodic disorders. Throughout the whole paper, we assume that $\alpha = (\sqrt{5} - 1)/2$. At the same time, we also introduced a slowly varying exponent v satisfying $0 < v < 1$. The introducing of slowly varying exponent breaks the \mathcal{PT} symmetry. If $V_{n,A} = V_{n,B} = 0$, then the model returns to the standard Hermitian SSH model. If we set $\lambda = 0$, Eq. (1) becomes a non-Hermitian AA model with slowly varying quasiperiodic disorders. This special case will also be studied in later sections.

To achieve slow varying, we always assume that $0 < v < 1$. With this condition, it is easy to see that the derivatives of the potential $V_{n,A}$ approach zero as the site index becomes very large as

$$\lim_{n \rightarrow \infty} \frac{dV_{n,A}}{dn} = \lim_{n \rightarrow \infty} i2\pi\alpha v n^{v-1} V e^{i(2\pi\alpha n^v)} = 0. \quad (3)$$

A similar result is also valid for $V_{n,B}$. This indicates that the quasiperiodic potential approaches a constant when the number of lattice sites of the model become very large. However, for a given finite-sized model, this constant is not unique and varies within a certain range depending on the system size. Because of this behavior, we claim that this model contains slowly varying quasiperiodic disorders. The existence of this slowly varying quasiperiodic disorders makes the appearance of the mobility edge possible in our model even without \mathcal{PT} symmetry.

In this paper, we mainly focus on the NH-SSH model of Eq. (1). We find that the property of supporting mobility edges can also be generalized to more complicated models. For a slowly varying disordered non-Hermitian model, if its unit cell contains even number of orbital, its qualitative behaviors are similar to the NH-SSH model. There will be clear mobility edges for suitable choices of parameters. However, if the unit cell contains odd number of orbital, there is no well defined mobility edges. The reason will be explained in the end of Sec. III A.

III. MOBILITY EDGES OF THE NON-HERMITIAN SSH MODEL

A. Determine the mobility edges by energy matching method

In this subsection, we will present a heuristic method called ‘‘energy matching method’’ [44], which can efficiently determine the mobility edges in Hermitian slowly varying quasiperiodic models. With some refinement, we find that this method is also applicable for the NH-SSH model. In addition, it can provide some clue for what type of slowly varying quasiperiodic models can support mobility edges when generalized to non-Hermitian systems. The core idea of this method is to make use the characteristics of slowly varying quasiperiodic potential that approaches to a constant at very large site index. Because of this, we can approximate the slowly varying quasiperiodic disordered model by a set of periodic models. The approximated periodic model Hamiltonian can be expressed as follows:

$$\hat{H} = \sum_{n=1}^{L/2} [(t_1 \hat{c}_{n,A}^\dagger \hat{c}_{n,B} + t_2 \hat{c}_{n,B}^\dagger \hat{c}_{n+1,A} + \text{H.c.}) + V_M \hat{c}_{n,A}^\dagger \hat{c}_{n,A} + V_M^* \hat{c}_{n,B}^\dagger \hat{c}_{n,B}]. \quad (4)$$

Here $V_M = V e^{i(2\pi\alpha M^v)}$ and V_M^* is the complex conjugate of V_M . For a fixed M , the potential is constant, therefore \hat{H}_M describes a periodic model. To reflect the quasiperiodic disorders of original model, we allow M to take all integer values between 1 and L . For convenience, we set $2\pi\alpha M^v = \phi$. It is obvious that the above periodic Hamiltonian has no non-Hermitian skin effect. Therefore all the eigenstates of the above periodic models are extended.

For these periodic model of Eq. (4), we can diagonalize the Hamiltonian by transferring to the momentum space, and find out that energy bands are given by

$$E = V \cos \phi \pm \sqrt{t_1^2 + t_2^2 + 2t_1 t_2 \cos k - V^2 \sin^2 \phi}. \quad (5)$$

For a given periodic model, the eigenstates with the energy inside the band are all extended. Here, we will focus on the intersection of the energy bands of all the periodic models. As we discussed before, the quasiperiodic model can be thought as a combination of all these periodic modes in some sense. Therefore, if the eigenenergy of the quasiperiodic model fall within the range of the above intersection, we can expect that the corresponding eigenstates to be extended. The region of extended states is obtained by matching their eigenenergy to the bands of periodic models. Therefore, it is dubbed as the “energy-matching method.” Since $|\cos k| < 1$, the energy region of the extended state is given by the following intersection:

$$E \in \bigcap_a (V \cos \phi + \sqrt{(2\lambda)^2 - V^2 \sin^2 \phi}, V \cos \phi + \sqrt{(2t)^2 - V^2 \sin^2 \phi}). \quad (6)$$

Here we only discuss the extended states region from the plus sign of Eq. (5). For the minus sign, the discussion is very similar. For Hermitian systems, the energy band of periodic models are real, thus the intersection of energy bands can be easily obtained. In contrast, for non-Hermitian systems, the energy bands of these periodic models can be complex, so the energy-matching method needs to be further refined before it can be applied to non-Hermitian quasiperiodic models.

We find that the energy bands of Eq. (5) can be divided into three different classes depending on the relative magnitude of V comparing to $2t$ and 2λ . Accordingly, the behavior of mobility edges of the NH-SSH model of Eq. (1) also falls into three classes. The details are explained as follows.

(1) When $V \leq 2\lambda$, no matter what value ϕ takes, the \mathcal{PT} symmetry of the periodic model is not broken and the energy bands of the periodic models are all real numbers. At this point, we can directly find the intersection of the energy bands of different \hat{H}_M , and the mobility edge is given by

$$E \in (2\lambda + V, 2t - V). \quad (7)$$

(2) When $2\lambda < V < 2t$, if ϕ satisfies $\phi > |\arcsin(2\lambda/V)|$, the \mathcal{PT} symmetry of the periodic model is broken, and the energy spectra of the periodic models have both real and complex values. Since $V < 2t$, we can see that the upper bounds of each energy band in Eq. (6) are still real numbers. However, since $V > 2\lambda$, the lower bounds of each energy band in Eq. (6) can become complex numbers. Since there is no natural order for complex numbers, one cannot determine the precise intersection of the lower bounds in Eq. (6). Instead, we can use the real parts of these complex eigenenergies to determine the lower bound as follows:

$$E \in \bigcap_a (\text{Re}[V \cos \phi + \sqrt{(2\lambda)^2 - V^2 \sin^2 \phi}], V \cos \phi + \sqrt{(2t)^2 - V^2 \sin^2 \phi}). \quad (8)$$

Then it is easy to find the region of extended states as

$$E \in (2\lambda + V, 2t - V). \quad (9)$$

The mobility edge obtained in this way seems to be the same as Eq. (7) of the type (1). However, the mobility edge in this

case is actually not completely correct because we only find the intersection of the real part of the complex eigenenergies and ignore the effects of the imaginary parts. We will demonstrate this inaccuracy by the numerical calculations in the next subsection.

(3) When $V \geq 2t$, if ϕ satisfies $\phi > |\arcsin(2t/V)|$, the \mathcal{PT} symmetry of the model is completely broken and all eigenenergies of the periodic models are complex. In addition, if we look for the intersection of the real parts of these complex energy bands, the result is an empty set. In other words, there are no longer extended states. Therefore, the mobility edges no longer exist in this case.

In the next subsection, the numerical calculations will be carried out to verify the mobility edges that are obtained by the above energy-matching method. These results also demonstrate that it is reasonable to divide the behaviors of mobility edges into three different classes.

Before we turn to the numerical verifications, we would like to discuss the application range of this energy matching method. Since this method is based on physical picture-like arguments rather than rigorous derivation, it is hard to give a precise application range of this method. According to our experience, the energy matching method can only apply to the non-Hermitian model with slowly varying quasiperiodic disorders. If the disorders of the non-Hermitian model are not slowly varying, the energy matching method usually cannot capture the mobility edges correctly.

The reason for this is that the energy matching method approximates the disordered model by a set of periodic models. For this approximation to be valid, the disorder potentials should be roughly like constants for a portion of lattice sites. This property is realized in the slowly varying disorders as the lattice site number j becomes large. For quasidisordered models without slowly varying, there is no such property, therefore, the energy matching does not work for this type of model.

Even for the slowly varying 1D models, the energy matching method can only be applied to a subclass of these models. If we consider a slowly varying disordered non-Hermitian model with an odd number of orbital in each unit cell, its approximated periodic models almost have no real spectra. This corresponds to the class (2) and (3) behaviors as we discussed before. Thus, we can deduce that there are no well-defined mobility edges for models with an odd number of orbital. Direct numerical calculations also support this conclusion.

B. Numerical results of the mobility edges

To demonstrate to what degree the eigenstates of the model localized, we make use of the inverse participate ratio (IPR) as the indicator of the localization [46,47]. For the m th normalized wave function ψ_m , the IPR is defined as follows:

$$\text{IPR}_m = \sum_{j=1}^L |a_j^m|^4, \quad \psi_m = (a_1^m, \dots, a_L^m). \quad (10)$$

Here L is the system size. It is well known that, for a generic extended state, the amplitude at each site should be roughly uniform. Therefore, if the eigenstate is extended, its IPR

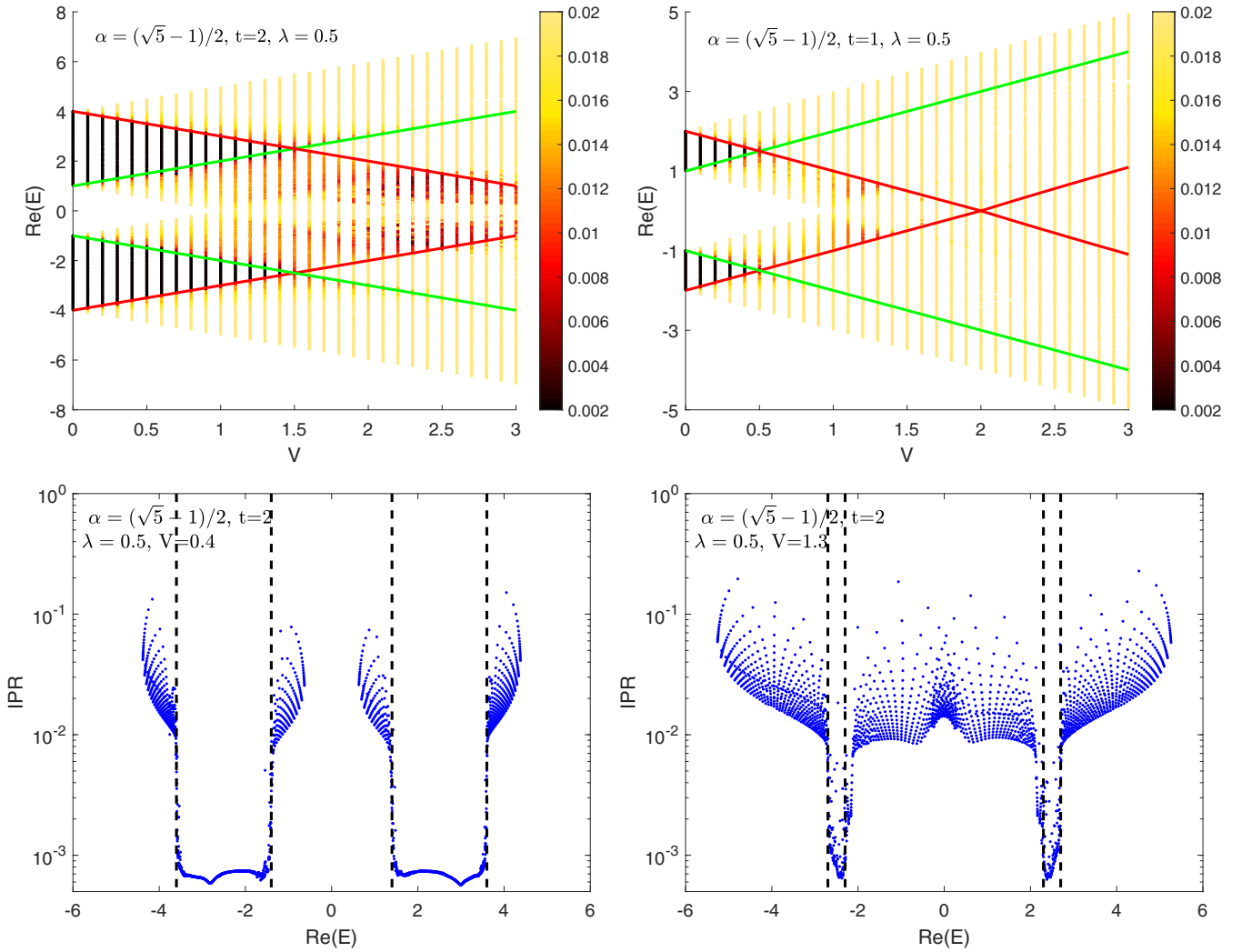


FIG. 2. Top row: The real parts of the energy band of Eq. (1) as a function of V . We assume that $t = 2$ (top left) and $t = 1$ (top right), respectively. The color of the point represents its IPR value. The red and green lines represents the mobility edges. Bottom row: The IPR as a function of the real part of eigenenergy. We assume $V = 0.4$ (bottom left) and $V = 1.3$ (bottom right), respectively. The dotted lines indicate the mobility edges. Other parameters used in calculations are $\alpha = (\sqrt{5} - 1)/2$, $v = 0.5$, $\lambda = 0.5$, and $L = 2000$.

should be close to

$$\sum_{j=1}^L (|a_j^m|^2)^2 \sim \sum_{j=1}^L \frac{1}{L^2} = \frac{1}{L},$$

which is close to 0 as $L \rightarrow \infty$. For a generic localized state, on the other hand, the amplitude will concentrate around a few particular sites. Therefore, one expected that the IPR of a localized state should be a number of order one.

We plot the real part of the energy band of Eq. (1) as a function of V in the top row of Fig. 2. The color of each point represent the IPR value of the corresponding eigenstate. The parameters used in the calculations are listed in the figure caption. The red and green lines are the mobility edges of Eq. (7) obtained by the energy matching method. It can be seen that these lines agree well with the separation boundary between dark colored and light colored areas in the figure. The dark and light colors correspond to the extended and the localized state regions, respectively.

It is useful to make a closer examination of the transition between the extended state and the localized state near the mobility edge. This can clearly demonstrate the differences among the three behaviors of the mobility edges discussed in the previous subsection. We plot the IPR as a function of the eigenenergy for two selected V in the bottom row of Fig. 2. In the bottom left panel, we choose $V = 0.4$ such that $V < 2\lambda$. In the bottom right panel, $V = 1.3$ satisfies $2\lambda < V < 2t$. From the bottom row of Fig. 2, we can clearly see that there is a significant jump of roughly 10^{-2} in the IPR values near the mobility edge, which shows the transition between the extended state and the localized state. It confirms the mobility edges in the pseudocolor plots in the top row of Fig. 2. In addition, one can see that there are some points in the extended state energy region that are significantly different from the IPR value of the extended state by the orders of magnitude in the bottom right panel of Fig. 2. These points are actually localized states. The existence of localized states inside the extended state region indicates that the mobility edge becomes

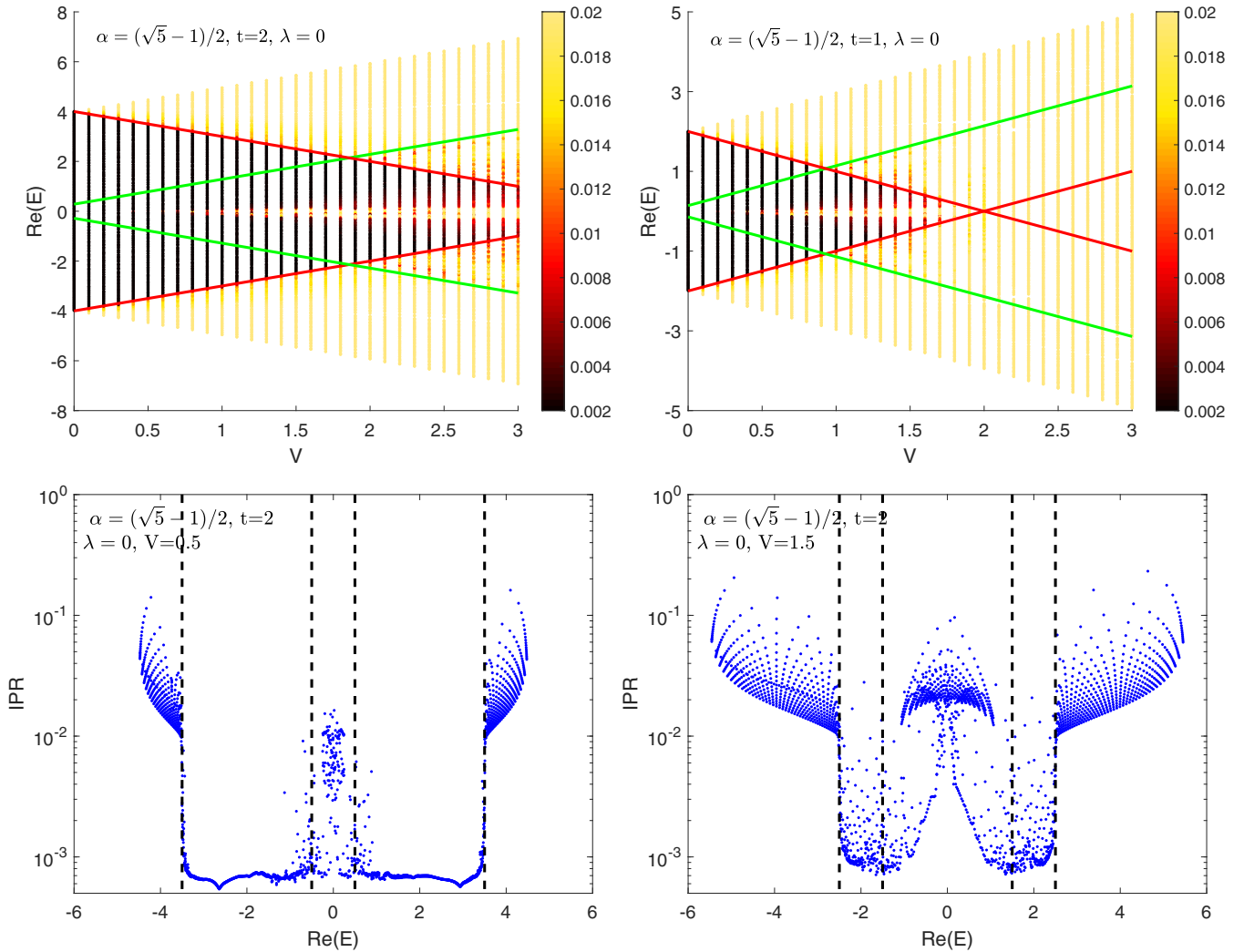


FIG. 3. Top row: The real parts of the energy band of Eq. (1) as a function of V with $\lambda = 0$. We assume that $t = 2$ (top left) and $t = 1$ (top right), respectively. The color of the point represents its IPR value. The red and green lines represents the mobility edges. Bottom row: The IPR as a function of the real part of eigenenergy. We assume $V = 0.5$ (bottom left) and $V = 1.5$ (bottom right), respectively. The dotted lines indicate the mobility edges. Other parameters are the same as in Fig. 2.

blurred, which is the signature of the second class that we discuss previously.

We would like to emphasize that the second class where $2\lambda < V < 2t$ is special for the slowly varying quasiperiodic non-Hermitian models. To take a closer look at this region, we set $\lambda = 0$, then the three classes of behaviors separated by 2λ and $2t$ collapses into two classes. First, when $V < 2t$, the eigenenergies of some periodic models in the energy-matching method are both real and complex. Second, for $V > 2t$, the eigenenergies of some periodic models are all complex numbers. We plot the real part of the energy band of Eq. (1) as a function of V for $t = 2$ (left) and $t = 1$ (right) in the top row of Fig. 3. Again, The color of the point represents its IPR value. One can see that the mobility edge obtained by the energy-matching method is not completely correct. More specifically, the mobility edge represented by the red lines correctly separate the localized states from the extended states. However, the green lines fail to do so. This is consistent with our previous analysis that the lower bound of the extended

states region does not exist due to the appearance of complex numbers eigenvalues. These complex eigenvalues invalidates the mobility edge obtained from the intersection of the lower bounds of Eq. (6).

Similarly, we plot the IPR as a function of the eigenenergy for two selected V in bottom row of Fig. 3. One can see that there is a clear transition between the extended states and the localized states near the red line (represented by the two outer dashed lines). However, the IPR values near the green line (represented by the two inner dashed lines) are quite chaotic. Therefore, the mobility edges corresponding to the green line are no longer valid, which is consistent with our previous analysis. Moreover, as V increases, the number of periodic models with complex eigenvalues also increases. This suggests that the mobility edges will become even more blurred as V increases. This behavior is also reflected in the bottom row of Fig. 3.

In the calculations of Figs. 2 and 3, we take the systems size to be $L = 2000$ which is large enough to show the feature

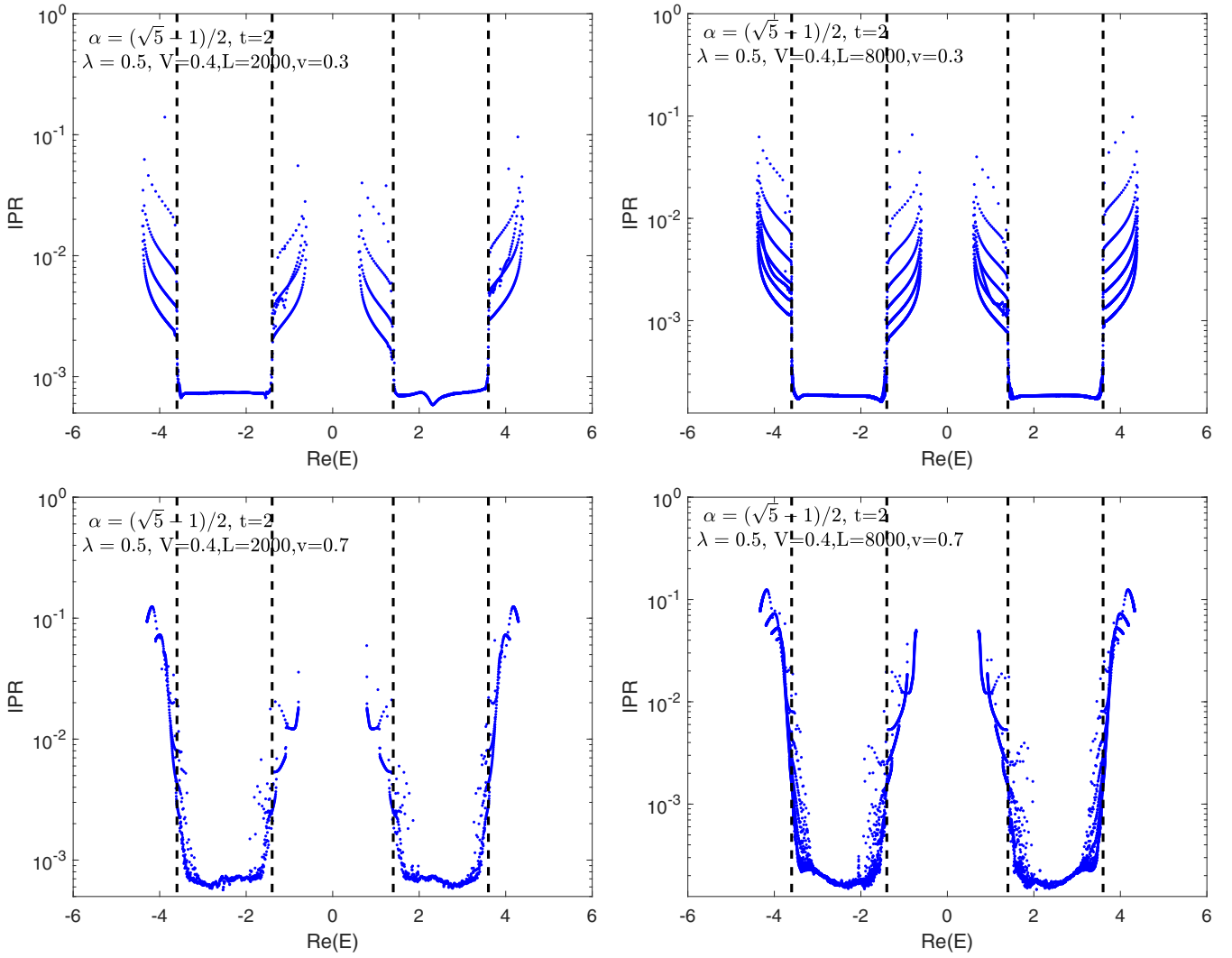


FIG. 4. The IPR as a function of the real part of eigenenergy of Eq. (1) for the slowly varying exponent $v = 0.3$ (top row) and $v = 0.7$ (bottom row). For the left two panels, the system size $L = 2000$. For the right two panels, $L = 8000$. The dashed line indicates the mobility edges. Other parameters are $V = 0.4$, $\alpha = (\sqrt{5} - 1)/2$, and $\lambda = 0.5$.

of slowly varying. These results should be roughly the same as the results of large L limit. For smaller L , the mobility edges will become blurred and there is no sharp boundary between localized and extended states. The finite-size effect of quasiperiodic models is discussed in [48]. To the best of our knowledge, there are no analytical results about the L dependence in slowly varying models.

At last, we want to demonstrate the effects of different slowly varying exponents v . In Fig. 4, we show the IPR values as a function of $\text{Re}(E)$ for the slowly varying exponent $v = 0.3$ (top row) and $v = 0.7$ (bottom row). For $v = 0.3$, one can see a sharp boundary between the zero and nonzero IPR values. Here the smaller v means that the disordered potentials approach to a constant at a faster rate than the case of $v = 0.5$. In this case, the extended states are more favorable than before and the mobility edges are well defined. On the other hand, for $v = 0.7$, the disordered potentials will approach a constant at a slower rate. The system favors the localized states and the mobility edges are slightly blurred. In the bottom right panel of Fig. 4, we increase the system size from $L = 2000$

to $L = 8000$. One can see the sharpness of mobility edges is slightly improved.

IV. WINDING NUMBERS OF THE NON-HERMITIAN SSH MODEL

For quasiperiodic non-Hermitian systems with \mathcal{PT} symmetry, the winding number is considered as an efficient tool to characterize the localization of the system. If the system is extended, the winding number is trivial $w = 0$. On the other hand, if the system is localized, it possess nontrivial winding numbers such as $w = \pm 1$. Therefore, we could also calculate the winding numbers for the model of Eq. (1) to investigate whether the model is localized or extended [49–54]. To define the winding number, we have to introduce an additional phase parameter θ into the potential of the model. More specifically, we can make the following replacement in Eq. (1):

$$V_{n,A} \rightarrow V e^{(i2\pi a n^v + i\frac{\theta}{L})}, \quad V_{n,B} \rightarrow V e^{(-i2\pi a n^v + i\frac{\theta}{L})}.$$

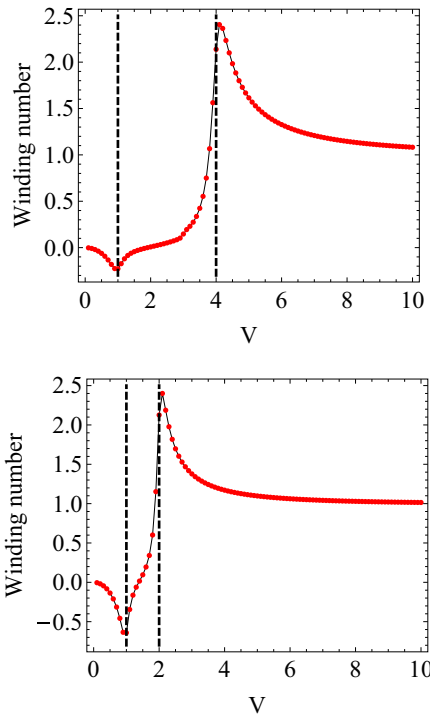


FIG. 5. The winding number for the model of Eq. (1) as a function of V with $t = 2$ (top) and $t = 1$ (bottom), respectively. Other parameters are $\lambda = 0.5$, $\alpha = (\sqrt{5} - 1)/2$, $v = 0.5$, and $L = 600$. The dotted lines are $V = 2\lambda$ and $V = 2t$.

Then we arrive at a Hamiltonian that depends on θ , which is denoted as $H(\theta/L)$. For a selected reference energy E_b , the winding numbers is defined as [16,23]

$$w(H) = \lim_{L \rightarrow \infty} \int_0^{2\pi} d\theta \frac{\partial}{\partial \theta} \log \det[H(\theta/L) - E_b]. \quad (11)$$

In our calculation, we set $E_b = 0$ since the spectra of Eq. (1) is almost symmetrically distributed around this point.

The intuitive picture of the winding number is to count how many times the complex energy spectrum of the model circles around the reference energy E_b , as θ increases from 0 to 2π . Usually, the winding number can serve as an indicator to the extended-localized transitions in non-Hermitian systems with \mathcal{PT} symmetry. This is because the localization transition in non-Hermitian model is often accompanied by the \mathcal{PT} symmetry breaking. Then the spectrum of the non-Hermitian model becomes complex and tends to exhibit a circular structure in the complex plane. Therefore, by observing whether the spectrum of the model exhibits a circular structure through the winding number, one can efficiently determine whether the system becomes localized. However, in our NH-SSH model, the \mathcal{PT} symmetry is explicitly broken by the slowly varying potentials. We will see that the winding number exhibits some new phenomena in our model.

In Fig. 5, we plot the winding number as a function of V for $t = 2$ (top) and $t = 1$ (bottom), respectively. It is evident that there are two singular points located at $V = 2\lambda$ and $V = 2t$ corresponding to the two dashed lines in the figure. One can see that the two singular points divide V axes into three parts, which agrees with the three types of behaviors of mobility

edges we discussed before. Here we can again use the energy-matching method to qualitatively understand the behavior of the winding number. The advantage of the approximation of Eq. (1) by a set of periodic models is that we have a simple expression Eq. (5) for the spectra of the periodic models.

For $V < 2\lambda$, the spectra of the approximated periodic models are all real. Therefore, in this case, the winding numbers is almost 0. Meanwhile, the intersection of all these bands give rise to the region of extended states. When V is close to the first singular point at 2λ , the winding number deviates from 0, which suggest some qualitative changes happen to the system around this point. When $2\lambda < V < 2t$, the spectra of the periodic models contains both real and complex eigenvalues. Accordingly, the winding numbers is not stable and rapidly increases from a very small value to a very large value. Meanwhile, the mobility edges become blurred in this case. When $V > 2t$, the spectra of the periodic models are all complex. Now the winding number decreases from the extreme large value and finally stabilizes to the quantized value 1. At the same time, the mobility edges disappear in this case, which means that all eigenstates are now localized. Therefore, the above three cases are consistent with the three types of behaviors of mobility edges.

We can also directly investigate how the spectra of Eq. (1) evolve with V . In Fig. 6, we plot the spectrum of Eq. (1) on the complex plane for $V = 0.6, 1.2$, and 4.8 , respectively. Due to the \mathcal{PT} symmetry breaking of this model, the spectra are all complex. On the top panel, the dashed lines indicate the mobility edges. Although the eigenenergy of the extended states are also complex, they are very close to the real axes. On the other hand, the spectra of the localized states are far more scattered. However, they are far from making a whole circle on the complex plane yet. Thus, the winding number is almost completely 0 for $V < 2\lambda$. As V increases to the range of $2\lambda < V < 2t$, the number of extended states decreases and the localized states start to dominate the spectra. However, their spectra still cannot make a full circle. As V further increases to $V > 2t$, the spectra of the localized states finally complete a whole circle, and the winding numbers eventually reach the quantized value 1.

We can also consider a special case by setting $\lambda = 0$. Then there is only one singularity point for the windings number curve, as shown in Fig. 7. This is consistent with previous analysis with $\lambda = 0$, where the behavior of mobility edges also falls into two cases: $V < 2t$ and $V > 2t$. In Fig. 8 we plot the spectrum of Eq. (1) with $\lambda = 0$ on the complex plane for $V = 1.2$ (top) and 4.8 (bottom). The spectra of the $V = 4.8$ case are almost the same as in the bottom panel of Fig. 6. However, the spectra of the $V = 1.2$ case of is far more scattered compared to the middle panel of Fig. 6. Due to $\lambda = 0$, the spectra already contain both real and complex eigenvalues in the range of $V < 2t$. Therefore, there are more localized states in this case, and this gives rise to more scattered spectra.

In summary, we found an intuitive relation between the mobility edges and the shape of spectra on the complex plane. If the spectra are roughly confined around the real axes, the extended states dominate the spectra and there exist sharp mobility edges. If the spectra are scattered, then the system is comprised of a mixture of both extended and localized states, and the mobility edges are blurred. If the spectra almost form a

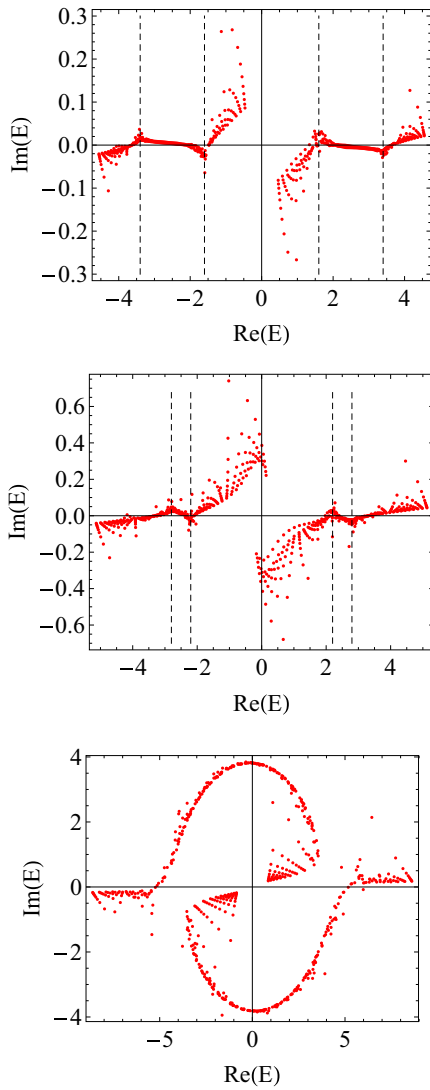


FIG. 6. The eigenenergy E of Eq. (1) plotted on the complex plane. From the top panel to the bottom panel, $V = 0.6, 1.2,$ and $4.8,$ respectively. The dashed lines represents the mobility edges. The parameters are the same as the top panel of Fig. 5.

circle around a fixed point, then the localized states dominate the system and there are no mobility edges.

At the end of this section, we briefly discuss a possible experimental realization of the model of Eq. (1). The one-dimensional quasiperiodic model can be realized by a discrete-time quantum walk of optical pulses [55–58]. The basic idea is to simulate the one-dimensional lattice by a sequence of pulses in the time domain. The initial optical pulse is sent into an interferometer with several unbalanced arms. Then a single pulse will split into several pulses with different time delays. The complex amplitudes of each pulse can be tuned by the electro-optic phase modulator (EOM) and an acoustooptic amplitude modulator (AOM) located at each arm. In this way, the amplitudes of these pulses will satisfy a linear equation, which can be chosen to be the eigenequation of the Hamiltonian of Eq. (1). If one iterates the above process many times, then a large sequence of pulses will be created. Their amplitude will also satisfy the eigenequation of the

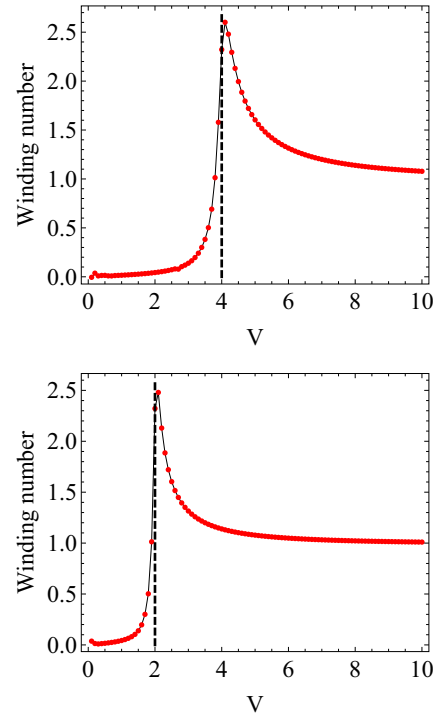


FIG. 7. The winding number for the model of Eq. (1) as a function of V with $t = 2$ (top) and $t = 1$ (bottom), respectively. Other parameters are $\lambda = 0, \alpha = (\sqrt{5} - 1)/2, v = 0.5,$ and $L = 300.$ The dotted lines are $V = 2\lambda$ and $V = 2t.$

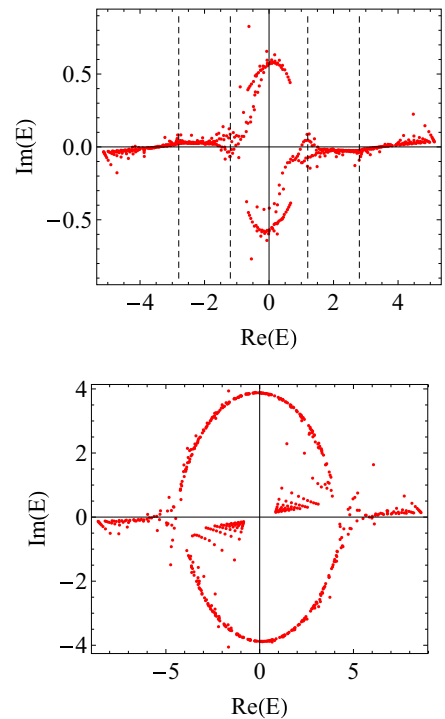


FIG. 8. The eigenenergy E of Eq. (1) plotted on the complex plane. From the top panel to the bottom panel, $V = 1.2$ and $4.8,$ respectively. The dashed lines represents the mobility edges. The parameters are the same as the top panel of Fig. 7.

given Hamiltonian. In principle, the slowly varying complex potential of Eq. (2) can also be realized by some suitable choices of amplitudes of EOM and AOM. A more detailed description of this type of experimental setup can also be found in [31].

V. CONCLUSION

As far as we know, most studies of non-Hermitian quasiperiodic disordered models focused on the disorders without slowly varying. In these models, the mobility edges were usually determined by duality transformations or real-complex transition of spectra. In contrast, for the slowly varying disordered non-Hermitian models, there are no duality transformations and their spectra are always complex. This means the two methods we just mentioned all fail for slowly varying models. For many slowly varying disordered non-Hermitian models, there are no clear mobility edges.

In this paper, we present an example of non-Hermitian model with slowly varying quasiperiodic disorders which can support well-defined mobility edges. We found that the behaviors of mobility edges fall into three classes depending on the amplitude of disorder potentials. These three classes also match with the winding number of the complex spectrum of the system. To understand these behaviors, we found that it is very useful to approximate the slowly varying model by a set of periodic models. This method is not only effective in determining the mobility edges in our example, it can also suggest a way to construct other slowly varying models to support mobility edges.

ACKNOWLEDGMENT

This work was supported by the Natural Science Foundation of China under Grant No. 11874272.

-
- [1] P. W. Anderson, *Phys. Rev.* **109**, 1492 (1958).
 - [2] E. Abrahams, P. W. Anderson, D. C. Licciardello, and T. V. Ramakrishnan, *Phys. Rev. Lett.* **42**, 673 (1979).
 - [3] P. A. Lee and T. V. Ramakrishnan, *Rev. Mod. Phys.* **57**, 287 (1985).
 - [4] N. Mott, *J. Phys. C: Solid State Phys.* **20**, 3075 (1987).
 - [5] P. G. H. Aubry and G. Andre, *Ann. Israel Phys. Soc.* **3**, 18 (1980).
 - [6] P. G. H. Aubry and G. Andre, *Proc. Phys. Soc. A* **68**, 874 (1955).
 - [7] J. Biddle and S. Das Sarma, *Phys. Rev. Lett.* **104**, 070601 (2010).
 - [8] S. Ganeshan, J. H. Pixley, and S. Das Sarma, *Phys. Rev. Lett.* **114**, 146601 (2015).
 - [9] F. M. Izrailev and A. A. Krokhin, *Phys. Rev. Lett.* **82**, 4062 (1999).
 - [10] J. Biddle, D. J. Priour, B. Wang, and S. Das Sarma, *Phys. Rev. B* **83**, 075105 (2011).
 - [11] S. Das Sarma, S. He, and X. C. Xie, *Phys. Rev. Lett.* **61**, 2144 (1988).
 - [12] S. Das Sarma, S. He, and X. C. Xie, *Phys. Rev. B* **41**, 5544 (1990).
 - [13] X. Li, X. P. Li, and S. Das Sarma, *Phys. Rev. B* **96**, 085119 (2017).
 - [14] X. Deng, S. Ray, S. Sinha, G. V. Shlyapnikov, and L. Santos, *Phys. Rev. Lett.* **123**, 025301 (2019).
 - [15] M. Saha, S. K. Maiti, and A. Purkayastha, *Phys. Rev. B* **100**, 174201 (2019).
 - [16] Z. Gong, Y. Ashida, K. Kawabata, K. Takasan, S. Higashikawa, and M. Ueda, *Phys. Rev. X* **8**, 031079 (2018).
 - [17] K. Kawabata, K. Shiozaki, M. Ueda, and M. Sato, *Phys. Rev. X* **9**, 041015 (2019).
 - [18] K. Esaki, M. Sato, K. Hasebe, and M. Kohmoto, *Phys. Rev. B* **84**, 205128 (2011).
 - [19] T. E. Lee, *Phys. Rev. Lett.* **116**, 133903 (2016).
 - [20] H. Shen, B. Zhen, and L. Fu, *Phys. Rev. Lett.* **120**, 146402 (2018).
 - [21] S. Yao and Z. Wang, *Phys. Rev. Lett.* **121**, 086803 (2018).
 - [22] A. Ghatak and T. Das, *J. Phys.: Condens. Matter* **31**, 263001 (2019).
 - [23] H. Jiang, L.-J. Lang, C. Yang, S.-L. Zhu, and S. Chen, *Phys. Rev. B* **100**, 054301 (2019).
 - [24] N. Hatano and D. R. Nelson, *Phys. Rev. Lett.* **77**, 570 (1996).
 - [25] N. Hatano and D. R. Nelson, *Phys. Rev. B* **58**, 8384 (1998).
 - [26] S. Longhi, *Phys. Rev. B* **100**, 125157 (2019).
 - [27] Q.-B. Zeng, S. Chen, and R. Lu, *Phys. Rev. A* **95**, 062118 (2017).
 - [28] Y. Liu, X.-P. Jiang, J. Cao, and S. Chen, *Phys. Rev. B* **101**, 174205 (2020).
 - [29] T. Liu and X. Xia, *Phys. Rev. B* **105**, 054201 (2022).
 - [30] C. Yuce and H. Ramezani, *Phys. Rev. B* **106**, 024202 (2022).
 - [31] T. Liu, H. Guo, Y. Pu, and S. Longhi, *Phys. Rev. B* **102**, 024205 (2020).
 - [32] X. Cai, *Phys. Rev. B* **103**, 214202 (2021).
 - [33] L.-Z. Tang, G.-Q. Zhang, L.-F. Zhang, and D.-W. Zhang, *Phys. Rev. A* **103**, 033325 (2021).
 - [34] A. Jazaeri and I. I. Satija, *Phys. Rev. E* **63**, 036222 (2001).
 - [35] Z. Xu, X. Xia, and S. Chen, *Phys. Rev. B* **104**, 224204 (2021).
 - [36] Y. Liu, Y. Wang, X.-J. Liu, Q. Zhou, and S. Chen, *Phys. Rev. B* **103**, 014203 (2021).
 - [37] X. Xia, K. Huang, S. Wang, and X. Li, *Phys. Rev. B* **105**, 014207 (2022).
 - [38] Y. Liu, Y. Wang, Z. Zheng, and S. Chen, *Phys. Rev. B* **103**, 134208 (2021).
 - [39] W. Chen, S. Cheng, J. Lin, R. Asgari, and G. Xianlong, *Phys. Rev. B* **106**, 144208 (2022).
 - [40] Z.-H. Wang, F. Xu, L. Li, D.-H. Xu, and B. Wang, *Phys. Rev. B* **105**, 024514 (2022).
 - [41] C.-X. Guo, X. Wang, H. Hu, and S. Chen, *Phys. Rev. B* **107**, 134121 (2023).
 - [42] S. Gopalakrishnan, *Phys. Rev. B* **96**, 054202 (2017).
 - [43] B. Zhu, R. Lu, and S. Chen, *Phys. Rev. A* **89**, 062102 (2014).
 - [44] Q. Tang and Y. He, *J. Phys.: Condens. Matter* **33**, 185505 (2021).
 - [45] Q. Tang and Y. He, *Chin. Phys. B* **32**, 127202 (2023).
 - [46] D. J. Thouless, *Phys. Rep.* **13**, 93 (1974).

- [47] M. Kohmoto, *Phys. Rev. Lett.* **51**, 1198 (1983).
- [48] Y. Wang, G. Xianlong, and S. Chen, *Eur. Phys. J. B* **90**, 215 (2017).
- [49] Q. B. Zeng and Y. Xu, *Phys. Rev. Res.* **2**, 033052 (2020).
- [50] W. Han and L. Zhou, *Phys. Rev. B* **105**, 054204 (2022).
- [51] X. Cai, *Phys. Rev. B* **103**, 014201 (2021).
- [52] X. Cai, *Phys. Rev. B* **106**, 214207 (2022).
- [53] L. Zhou, *Phys. Rev. B* **108**, 014202 (2023).
- [54] S. Longhi, *Phys. Rev. Lett.* **122**, 237601 (2019).
- [55] A. Schreiber, K. N. Cassemiro, V. Potoček, A. Gábris, P. J. Mosley, E. Andersson, I. Jex, and C. Silberhorn, *Phys. Rev. Lett.* **104**, 050502 (2010).
- [56] A. Schreiber, K. N. Cassemiro, V. Potoček, A. Gábris, I. Jex, and C. Silberhorn, *Phys. Rev. Lett.* **106**, 180403 (2011).
- [57] A. Regensburger, C. Bersch, B. Hinrichs, G. Onishchukov, A. Schreiber, C. Silberhorn, and U. Peschel, *Phys. Rev. Lett.* **107**, 233902 (2011).
- [58] S. Derevyanko, *Sci. Rep.* **9**, 12883 (2019).